Electronic Supplementary Material (ESI) for RSC Advances.


**Supporting Information**

# A SERS aptasensor for sensitive and selective detection of bis(2-ethylhexyl) phthalate

Dandan Tu [a,*], Javier T. Garza [a], and Gerard L. Coté [a,b]

[a] Department of Biomedical Engineering, Texas A&M University, College Station, Texas 77843, United States

[b] Center for Remote Health Technologies & Systems, Texas A&M Engineering Experiment Station, College Station, Texas 77843, United States

* Corresponding author at: Department of Biomedical Engineering, Texas A&M University, College Station, Texas 77843, USA. Tel.: +1 979 402 5853.

E-mail address: dandan_tu2016tamu@tamu.edu

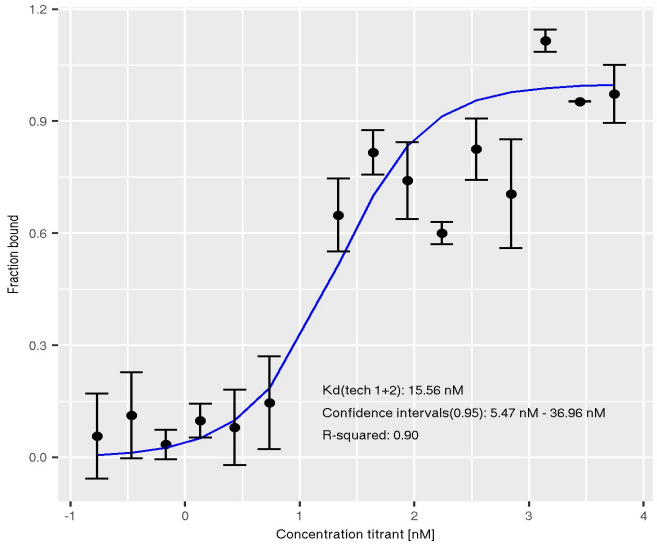


Fig. S1 Binding behavior of the DEHP aptamer to free DEHP molecules measured by microscale thermophoresis(MST). 170pM to 556μM of DEHP molecules were exposed to a constant concentration(10nM) of the DEHP aptamer. The fraction of the DEHP aptamer bound to the free DEHP molecule was plotted versus the titrated DEHP concentration. The dissociation constant $K_d$ is estimated to be 15.56nM. The error bars represent the standard deviation (SD) of three replicates (n=3).

A

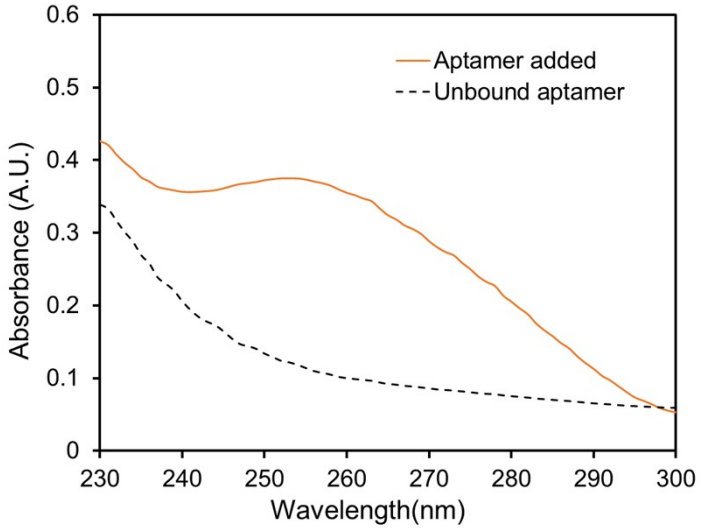


B

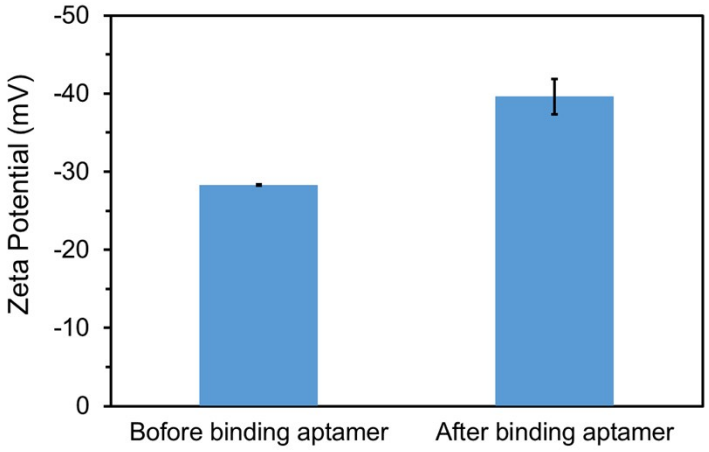


Fig. S2 (A) Absorbance spectra of the aptamer added into the magnetic beads, and the unbound aptamer left after magnetic separation. The concentration of the aptamer added was around 1.7μM, and the concentration of unbound aptamer was around 0.86nM. The aptamer concentration was calculated by Beer's law using the absorbance at 257nm, and the molar extinction coefficient of 323200 L•$mol^{-1}$•$cm^{-1}$. (B) ζ potential of the magnetic particle before and after aptamer modification. The error bars represent the SD of three replicates (n=3).

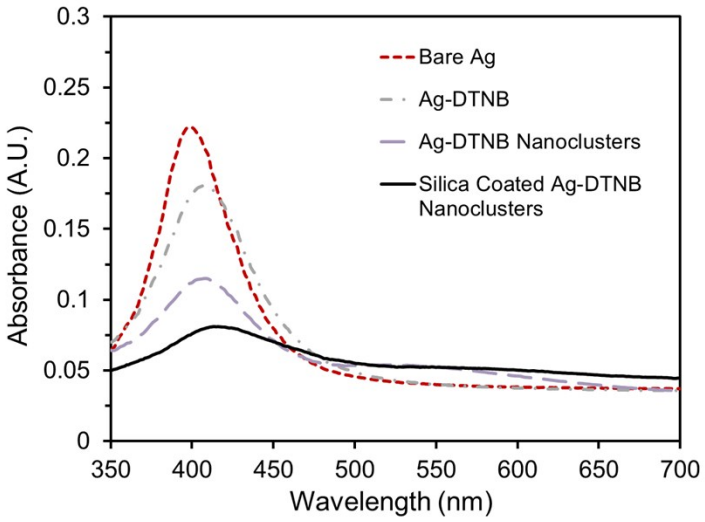


Fig.S3 UV-Vis spectra of bare silver nanoparticle, DTNB modified silver nanoparticles, silver nanoclusters, and silica coated silver nanoclusters.

In Fig.S3 a red shift in the SPR peak was observed for the Ag nanoparticles functionalized with DTNB as compared with bare Ag nanoparticles, indicating the attachment of DTNB on the nanoparticles. After introducing NaCl into the Ag-DTNB solution, silver nanoclusters formed, which caused a broad SPR band at ~522 nm. A red shift (~8 nm) could also be observed after coating the nanoclusters with silica. This occurred because the addition of a silica shell leads to an increase in local refractive index around the metal, which causes a red shift in the SPR peak [1, 2]. A large signal drop was also observed in the SPR peak near 414 nm, which was caused by the removal of silica coated silver monomers (~414 nm) in the washing step.

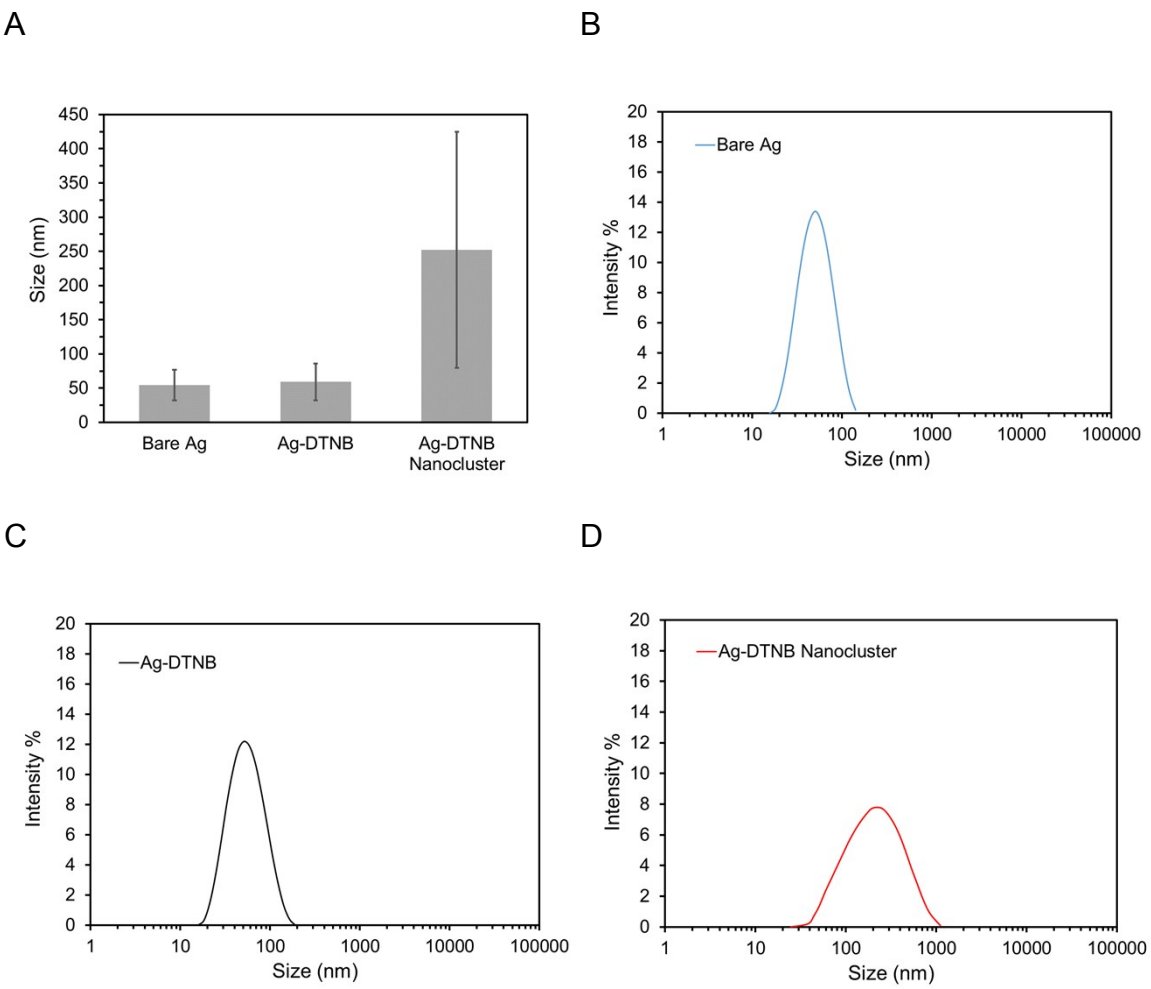


Fig. S4 (A) Hydrodynamic sizes of bare silver nanoparticles, DTNB modified silver nanoparticles, and silver nanoparticle clusters. Size distributions of (B) bare silver nanoparticles, (C) DTNB modified silver nanoparticles, and (D) silver nanoparticle clusters.

The hydrodynamic sizes of the nanoparticles were characterized by dynamic light scattering (DLS). The bare silver nanoparticles had an approximate size of 54.6 nm. After modification with DTNB, the size increased to 58.9 nm, suggesting the formation of a self-assembled monolayer (SAM) on the surface of the silver nanoparticles (Ag-DTNB). After clustering the Ag-DTNB nanoparticles using NaCl, the size increased, and the size distribution became broader. The

discrepancy between the sizes observed with the TEM and in the DLS is attributed to the fact that DLS measures the hydrodynamic size of the particle, and a few solvation layers are included in the measurement, leading to a larger size measured by the DLS [3].

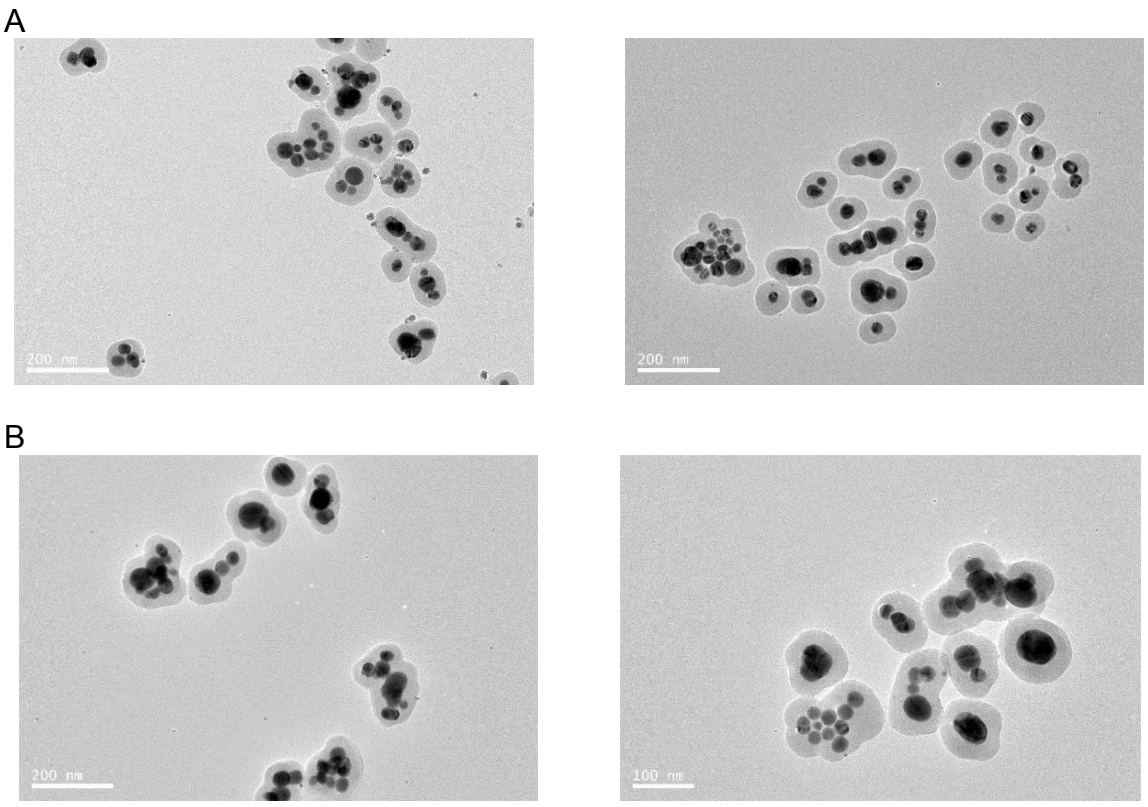


Fig. S5 TEM image of (A) the SERS silica particles before purification. (B) the SERS silica particles discarded in the purification process, which was composed of a large portion of large clusters (n≥4), and a small portion of monomers, dimers, and trimers.

As the salt induced clustering of nanoparticles is a random aggregation process, clusters composed of different number of nanoparticles could be formed [4]. As can be observed in Fig. S5A, there were monomers, dimers, trimers, and large clusters with more than 4 nanoparticles ($n \geq 4$) in the tested solution. Because the number of nanoparticles in the cluster can affect the consistency of the SERS intensity and the size of the silica particle, which can affect the binding process with the aptamer, it is necessary to separate nanoclusters with specific numbers of particles to get a more uniform SERS signal. Thus, a purification step was applied to separate nanoclusters with specific numbers of particles. Most of the small clusters ($n=2$ and 3) could be separated from the large clusters ($n \geq 4$) by collecting the supernatant after centrifugation (×600 g, 5 min). TEM images of the pellet discarded in the purification process (Fig. S5B) demonstrated that the removed particles were mostly large nanoclusters. It can be seen in Fig. 3A that the purified SERS silica particles are composed of dimers, trimers, and some monomers, indicating a good isolation of the small clusters ($n=2$ and 3).

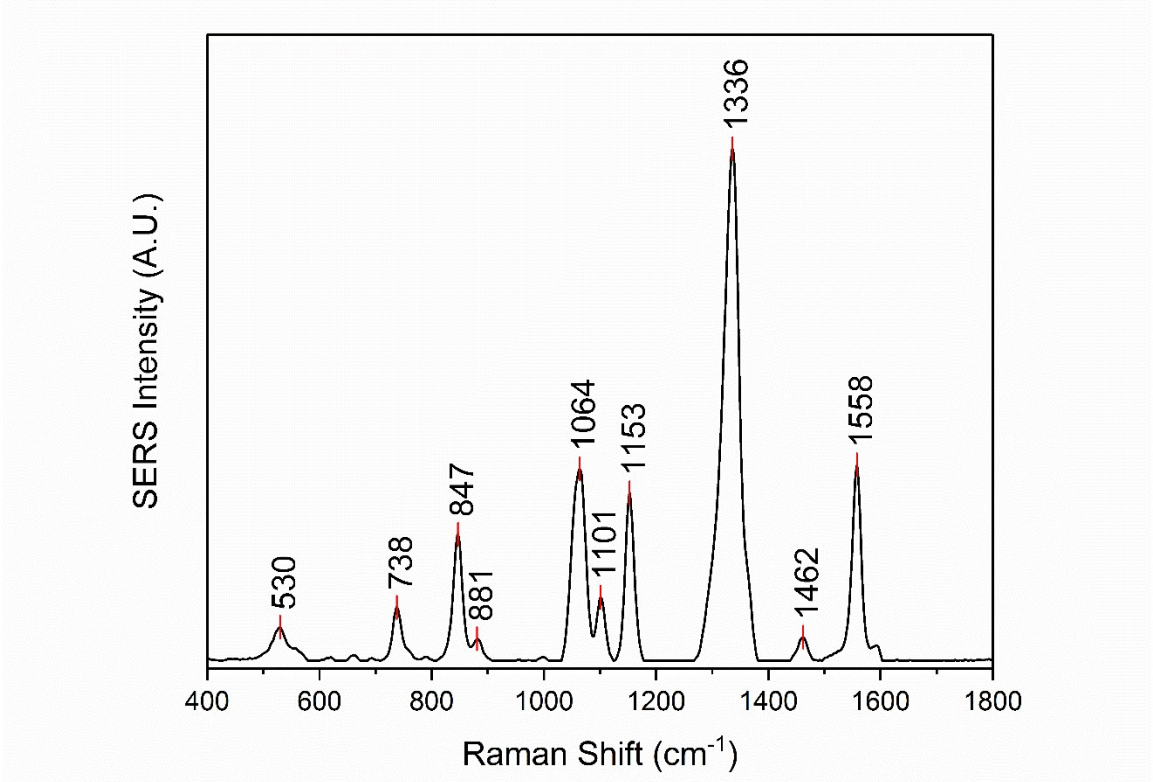


Fig. S6 SERS signals of the SERS silica particles in solution. The spectrum corresponds to DTNB, which is the Raman reporter molecule.

Table S1. Assignment of DTNB vibrational modes to the SERS spectrum of the SERS silica particles.

| Peak ($cm^{-1}$) | Assignment | Reference |
|---|---|---|
| 1558 | Aromatic ring stretching | [5, 6] |
| 1336 | Symmetric stretch of the N–O nitro group | [5-7] |
| 1064 | Succinimidyl N–C–O stretch overlapping with aromatic ring modes | [6, 8] |
| 847 | Nitro scissoring vibration | [6] |

Table S2. SERS silica particles signal mean, standard deviation, and coefficient of variation (CV) for three replicates.

| SERS Silica Particles Concentration (M) | Mean (Value at 1336cm$^{-1}$) | Standard Deviation | CV(%) |
|---|---|---|---|
| 2.80E-11 | 3072.45 | 34.26 | 1.11% |
| 2.10E-11 | 2217.43 | 37.49 | 1.69% |
| 1.12E-11 | 1476.90 | 30.65 | 2.08% |
| 5.60E-12 | 759.08 | 11.37 | 1.50% |
| 2.80E-12 | 366.78 | 21.00 | 5.73% |
| 1.40E-12 | 197.63 | 8.25 | 4.18% |
| 7.00E-13 | 108.74 | 7.04 | 6.47% |
| 2.80E-13 | 41.94 | 2.75 | 6.55% |

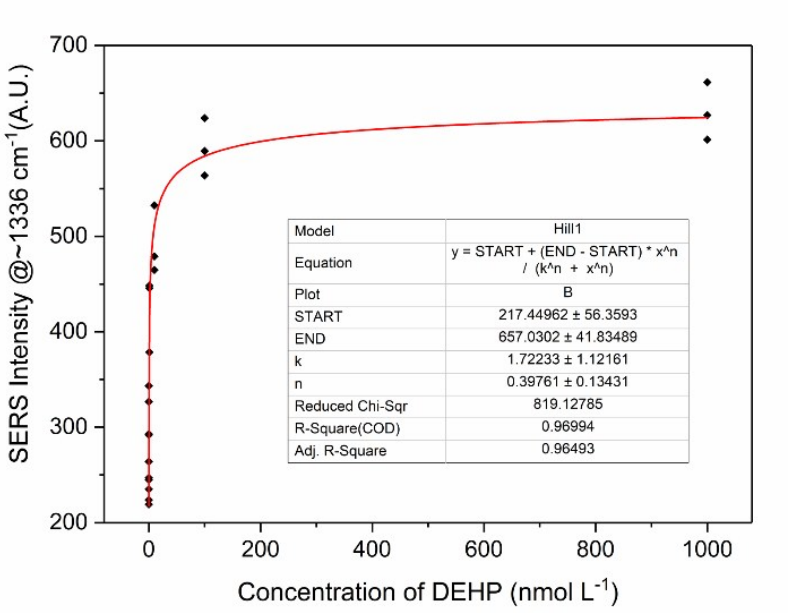


Fig. S7 The data points represent the SERS peak intensities at ~1336 $cm^{-1}$ for different concentrations of DEHP. The solid line is the fit line of the data points using the Hill equation, and the inset table shows the parameters of the Hill equation used to fit the response curve.

As shown in Fig. S7, modified Hill function was used to fit the response data. The fitted model was $y = 217.44 + \frac{(657.03 - 217.45) * x^{0.40}}{1.72^{0.40} + x^{0.40}}$. Using the $3\sigma$ method, LOD was obtained by adding 3 times the SD to the blank response (y=231.35+3*10.82=263.81), and then calculating the concentration that corresponds to the response signal using the fitted model (x=8 pM). Thus, the LOD of the DEHP aptasensor is 8 pM.

By calculating the lower limit of detection (LLOD) and the upper limit of detection (ULOD), the analytical range could be determined. The LLOD was calculated by plugging the response of 0 nM DEHP plus 3σ (i.e. Min+3σ) in the

fitted model. Specifically, using y=231.35+3*10.82=263.81 and inputting this value in the model, the LLOD value was calculated to be 0.008 nM. The ULOD was calculated by plugging the response of highest concentration of DEHP minus 3σ (i.e. Max-3σ) in the fitted model. Specifically, the response of 1000nM DEHP with a mean value of 629.93 was used. By plugging y=629.93-3*10.82=597.47 in the model, ULOD value was determined to be 182 nM. Thus, the analytical range of the aptasensor is 0.008 nM to 182 nM.

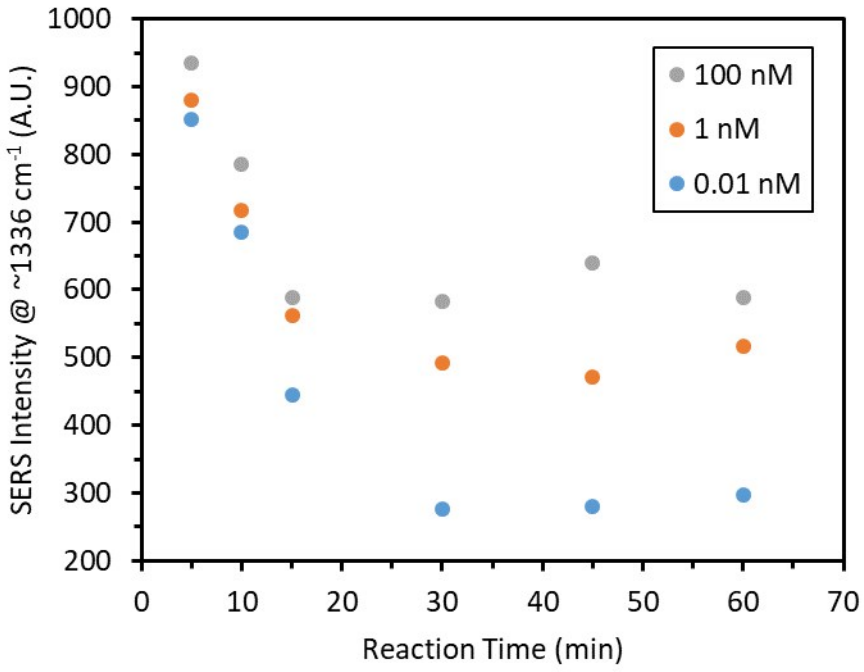


Fig. S8 The time response of the designed DEHP assay after exposure to 0.01 nM, 1 nM, and 100 nM of the analyte DEHP.

SERS silica particles and 100 nM DEHP sample were mixed with magnetic particles. Six wells of the mixtures were made and then incubated for 5 mins, 10

mins, 15mins, 30mins, 45mins, and 60 mins, respectively. After incubation, the particles were separated using a magnet. Subsequently, the supernatant of each mixture was collected and the SERS signal was measured using a portable Raman spectrometer. A similar process was repeated for 1 nM and 0.01 nM of DEHP. The result is shown in Fig. S8. From Fig. S8 it can be seen that the response is still not stable when the reaction time is shorter than 30 mins. From 30 mins to 60 mins, the reaction is fairly stable. Since waiting 30 mins ensures that the assay reacts completely, it was decided to wait 30 mins for the reaction time.

Table S3. Summary of other sensors for detection of DEHP.

| | Detection Method | Dynamic Range (nM) | LOD (pM) | Year | References |
|---|---|---|---|---|---|
| **Immunosensor** | An ELISA assay | 12.8 - 256 | 256 | 2017 | [9] |
| | A direct competitive enzyme-linked immunosorbent assay | 0.003 - 2560 | 10.8 | 2015 | [10] |
| | An indirect competitive biotin–streptavidin enzyme-linked immunosorbent assay | 0.053 - 33 | 18.9 | 2014 | [11] |
| **Aptasensor** | A signaling-probe displaced electrochemical aptamer based biosensor | 0.01 - 100 | 10 | 2017 | [12] |
| **Other type** | An electrochemical sensor using ferrocene-terminated poly(amine) ester dendrimer-GO modified glassy carbon electrodes (Fc-AED/GO/GCE) | 600 - $10^6$ | $9\times10^5$ | 2018 | [13] |
| | An extended gate organic field effect transistor (EG-OFET) with the extended gate coated with molecularly imprinted polymer (MIP) | 64 - 128 | - | 2018 | [14] |
| | An electrochemical sensor using a glassy carbon electrode modified with β-cyclodextrin/graphene/1,10-diaminodecane (β-CD–G–DAD) composite | 200 - 1200 | $1\times10^4$ | 2015 | [15] |
| | A planar interdigital sensor with a sensing surface functionalized by a self-assembled monolayer of 3-aminopropyltrietoxysilane (APTES) with embedded molecular imprinted polymer (MIP) | 2560 - $2.6\times10^5$ | - | 2015 | [16] |
| | A method combined membrane filtration-enrichment with diffuse reflectance UV (DRUV) spectroscopy | 77- 1792 and 2560 - 12802 | 20227 | 2014 | [17] |
| | An electrochemical sensor using β-cyclodextrin-graphene hybrid composites modified glassy carbon electrode | 2000 -18000 | $1.2\times10^5$ | 2014 | [18] |

# References


[1] Li, H.Q., Deng, Q.Q., Liu, B., Yang, J.H., and Wu, B., Fabrication of core@spacer@shell Au-nanorod@mSiO(2)@Y2O3:Er nanocomposites with enhanced upconversion fluorescence. Rsc Advances, 2016. **6**(16): p. 13343-13348.

[2] Das, M., Yi, D.K., and An, S.S.A., Analyses of protein corona on bare and silica-coated gold nanorods against four mammalian cells. International Journal of Nanomedicine, 2015. **10**: p. 1521-1545.

[3] Olariu, C.I., Yiu, H.H.P., Bouffier, L., Nedjadi, T., Costello, E., Williams, S.R., Halloran, C.M., and Rosseinsky, M.J., Multifunctional Fe3O4 nanoparticles for targeted bi-modal imaging of pancreatic cancer. Journal of Materials Chemistry, 2011. **21**(34): p. 12650-12659.

[4] Chen, G., Wang, Y., Tan, L.H., Yang, M., Tan, L.S., Chen, Y., and Chen, H., High-purity separation of gold nanoparticle dimers and trimers. J Am Chem Soc, 2009. **131**(12): p. 4218-9.

[5] Lin, C.C. and Chang, C.W., AuNPs@mesoSiO2 composites for SERS detection of DTNB molecule. Biosens Bioelectron, 2014. **51**: p. 297-303.

[6] Wang, Z., Zong, S., Yang, J., Li, J., and Cui, Y., Dual-mode probe based on mesoporous silica coated gold nanorods for targeting cancer cells. Biosens Bioelectron, 2011. **26**(6): p. 2883-9.

[7] Schutz, M., Kustner, B., Bauer, M., Schmuck, C., and Schlucker, S., Synthesis of glass-coated SERS nanoparticle probes via SAMs with terminal SiO2 precursors. Small, 2010. **6**(6): p. 733-7.

[8] Shrestha, Y.K. and Yan, F., Determination of critical micelle concentration of cationic surfactants by surface-enhanced Raman scattering. Rsc Advances, 2014. **4**(70): p. 37274-37277.

[9] Fang, H.Q., Wang, J., and Lynch, R.A., Migration of di(2-ethylhexyl)phthalate (DEHP) and di-n-butylphthalate (DBP) from polypropylene food containers. Food Control, 2017. **73**: p. 1298-1302.

[10] Zhang, M.C., Hong, W.T., Wu, X.Y., Zhang, Y., Li, F.Z., and Zhao, S.Q., A highly sensitive and direct competitive enzyme-linked immunosorbent assay for the detection of di-(2-ethylhexyl) phthalate (DEHP) in infant supplies. Analytical Methods, 2015. **7**(13): p. 5441-5446.

[11] Sun, R.Y. and Zhuang, H.S., A sensitive heterogeneous biotin-streptavidin enzyme-linked immunosorbent assay for the determination of di-(2-ethylhexyl)phthalate (DEHP) in beverages using a specific polyclonal antibody. Analytical Methods, 2014. **6**(24): p. 9807-9815.

[12] Han, Y., Diao, D.L., Lu, Z.W., Li, X.N., Guo, Q., Huo, Y.M., Xu, Q., Li, Y.S., Cao, S.L., Wang, J.C., Wang, Y., Zhao, J.X., Li, Z.F., He, M., Luo, Z.F., and Lou, X.H., Selection of Group-Specific Phthalic Acid Esters Binding DNA Aptamers via Rationally Designed Target Immobilization and Applications for Ultrasensitive and Highly Selective Detection of Phthalic Acid Esters. Analytical Chemistry, 2017. **89**(10): p. 5270-5277.

[13] Xiao, F.J., Guo, M.Y., Wang, J.Z., Yan, X.R., Li, H.L., Qian, C., Yu, Y.J., and Dai, D.Y., Ferrocene-terminated dendrimer functionalized graphene oxide layered sensor toward highly sensitive evaluation of Di(2-ethylhexyl) phthalate in liquor samples. Analytica Chimica Acta, 2018. **1043**: p. 35-44.

[14] Venkatesh, S., Yeung, C.C., Sun, Q.J., Zhuang, J.Q., Li, T., Li, R.K.Y., and Roy, V.A.L., Selective and sensitive onsite detection of phthalates in common solvents. Sensors and Actuators B-Chemical, 2018. **259**: p. 650-657.

[15] Xiong, S.Q., Cheng, J.J., He, L.L., Cai, D.Q., Zhang, X., and Wu, Z.Y., Fabrication of beta-cyclodextrin/graphene/1,10-diaminodecane composite on glassy carbon electrode and impedimetric method for Di(2-ethyl hexyl) phthalate determination. Journal of Electroanalytical Chemistry, 2015. **743**: p. 18-24.

[16] Zia, A.I., Mukhopadhyay, S.C., Yu, P.L., Al-Bahadly, I.H., Gooneratne, C.P., and Kosel, J.,

Rapid and molecular selective electrochemical sensing of phthalates in aqueous solution. Biosensors & Bioelectronics, 2015. **67**: p. 342-349.
[17] Chen, G.P., Hu, H.L., Wu, T., Tong, P.J., Liu, B.X., Zhu, B.L., and Du, Y.P., Rapid and sensitive determination of plasticizer diethylhexyl phthalate in drink by diffuse reflectance UV spectroscopy coupled with membrane filtration. Food Control, 2014. **35**(1): p. 218-222.
[18] Xiong, S.Q., Cheng, J.J., He, L.L., Wang, M., Zhang, X., and Wu, Z.Y., Detection of di(2-ethylhexyl) phthalate through graphene-beta-cyclodextrin composites by electrochemical impedance spectroscopy. Analytical Methods, 2014. **6**(6): p. 1736-1742.